

1 **The source of Dalradian detritus in the Buchan Block, NE Scotland:**  
2 **application of new tools to detrital datasets**

3

4

5 **T. E. Johnson<sup>1\*</sup>, C. L. Kirkland<sup>1</sup>, S. M. Reddy<sup>1</sup>, N. J. Evans<sup>1</sup> & B. J. McDonald<sup>1</sup>**

6

7

8

9 <sup>1</sup> *Department of Applied Geology, The Institute for Geoscience Research (TIGeR), Curtin*

10 *University, GPO Box U1987, Perth WA 6845, Australia (tim.johnson@curtin.edu.au)*

11

12

13

14

15 Short title: **Detrital zircon ages in the Buchan Block**

16 **ABSTRACT**

17

18 Detrital zircon from four samples of upper Dalradian metasedimentary rocks from the Buchan  
19 Block in the NE Grampian Highlands of Scotland were analysed by laser ablation inductively  
20 coupled mass spectrometry to establish their U–Pb age and trace element composition. The  
21 analysed grains (magmatic cores) mainly yield concordant ages ranging from Neoproterozoic to  
22 Eoarchaean. Kernel density plots of the data show pronounced peaks in the late  
23 Mesoproterozoic, Paleoproterozoic and Neoproterozoic eras. The data are indistinguishable from  
24 detrital zircon age spectra from Dalradian rocks elsewhere, an interpretation supported by  
25 application of a non-parametric multidimensional scaling algorithm, and are consistent with a  
26 Laurentian source. Similar to existing studies from other Dalradian rocks, the age spectra from  
27 the Buchan Block reveals an increase in the relative proportion of older detritus with time,  
28 suggesting derivation from late Mesoproterozoic (Grenville) then Palaeoproterozoic orogens  
29 before widespread exposure and denudation of their Archaean basement rocks. Application of a  
30 novel approach to estimate the most likely time of radiogenic-Pb loss indicates some detrital  
31 zircon grains were affected by element mobility around 470–450 Ma as a result of Grampian  
32 orogenesis.

33

34

35 Supplementary materials: Laser ablation inductively coupled mass spectrometry U–Pb and trace  
36 element data, a matrix showing results of Kolmogorov–Smirnov (K–S) test,  
37 cathodoluminescence imaging of zircons and selected trace element plots are available at  
38 <https://doi.org/10.1017/S0007152820000000>.

39

40

41 **Key words:** Buchan Block, Dalradian, U–Pb detrital zircon age, Laurentia, provenance.

## 42 INTRODUCTION

43  
44 The Dalradian Supergroup of Scotland and Ireland is a thick sequence of Neoproterozoic to  
45 lower Palaeozoic rocks that were deposited along the eastern margin of Laurentia, then deformed  
46 and metamorphosed during the complex Cambrian to Devonian Caledonian orogenic cycle,  
47 during the opening and subsequent closure of the Iapetus Ocean (McKerrow et al. 2000; Chew  
48 and Strachan 2014). The rocks have a long history of research dating back to Hutton's *Theory of*  
49 *the Earth* (1788), and have been key to the development of many fundamental geological  
50 concepts (see Stephenson et al. (2013a) and references therein).

51         The absolute age and age distribution of detrital minerals is a proven tool in constraining  
52 the source and depositional age of siliciclastic rocks, which may provide critical information on  
53 larger scale models of crustal evolution (Košler et al. 2002; Andersen 2005; Cawood et al.  
54 2012b, 2013; Spencer and Kirkland 2015). Much of the Dalradian Supergroup records the legacy  
55 of sedimentary basins formed during the Neoproterozoic era, a dynamic period in Earth history  
56 where climactic extremes may have been the environmental forcing that spawned complex life  
57 (Hoffman and Schrag 2002; Prave et al. 2009). However, of the published detrital zircon age  
58 data from (meta)sedimentary rocks from the Dalradian Supergroup (Cawood et al. 2003; Banks  
59 et al. 2007; Chew et al. 2009, 2010; McAteer et al. 2010b; Strachan et al. 2013), there are none  
60 from the Buchan Block, a structurally-bound package of upper Dalradian Supergroup rocks in  
61 north-east Scotland that exhibits profound differences in its sedimentological, structural,  
62 magmatic and metamorphic history when compared to the rest of the Grampian Terrane (Figs 1  
63 & 2). These differences have led some workers to regard the Buchan Block as an allochthonous  
64 crustal terrane comprising pre-Caledonian basement gneisses and cover rocks that were thrust  
65 into their current position during the Grampian phase of Caledonian orogenesis (Sturt et al.  
66 1977; Ramsay and Sturt 1978).

67 Here we present laser ablation inductively coupled mass spectrometer (LA–ICP–MS) U–  
68 Pb age and rare earth element (REE) data from detrital zircons in four metasedimentary rocks  
69 from the Buchan Block. These data are compared with existing data from Dalradian Supergroup  
70 rocks with the aim of better understanding the age and source of detritus within the Buchan  
71 Block.

72

73

## 74 **REGIONAL GEOLOGY**

75

76 The Grampian Terrane, comprising the Dalradian Supergroup, its basement and intrusive  
77 rocks, is one of several major crustal blocks that amalgamated to form the northern part of the  
78 British Isles. It comprises a NE–SW-trending belt of rocks that extends from the Shetland  
79 Islands through the highlands of Scotland and into northern and northwestern Ireland, and is  
80 bound to the north by the Great Glen Fault and to the south by the Highland Boundary Fault–  
81 Fair Head–Clew Bay Line (Fig. 1). The rocks record a complex sequence of tectonomagmatic  
82 events, termed the Caledonian orogenic cycle (McKerrow et al. 2000; Chew and Strachan 2014),  
83 related to the opening and closure of the Iapetus Ocean during supercontinent breakup and  
84 reassembly in the lower Palaeozoic (Cambrian to Devonian) (Soper 1994; Dewey and Mange  
85 1999; Cawood et al. 2003, 2007a; Chew et al. 2009; Kirkland et al. 2013; Chew and Strachan  
86 2014). Recent reviews on the Caledonides of Scotland and Ireland are provided by Stephenson et  
87 al. (2013a), Chew and Strachan (2014), Tanner (2014) and Dewey et al. (2015), and of the  
88 geology of the north-east Grampian Highlands, including the Buchan Block, by Stephenson et al.  
89 (2013b).

90 The dominant component of the Grampian Terrane is the mid-Neoproterozoic to early  
91 Palaeozoic Dalradian Supergroup, a sequence of deformed and metamorphosed rocks dominated  
92 by marine siliclastic rocks with some carbonate and volcanic units that are intruded by pre- to

93 post-orogenic igneous bodies ranging from peridotite to granite. From base to top, the Dalradian  
94 Supergroup comprises the Grampian, Appin, Argyll and Southern Highland Groups, which have  
95 a total aggregate thickness in the order of 20–25 km (Harris 1994; Stephenson et al. 2013a).  
96 Deposition of the Dalradian Supergroup probably commenced at around 730 Ma and continued  
97 until c.520–510 Ma (Tanner and Pringle 1999; Tanner and Sutherland 2007; Stephenson et al.  
98 2013a), although these ages are debated and the base of the succession may be older than 800  
99 Ma (Prave et al. 2009).

100         At the base of the Dalradian Supergroup in Scotland, the Grampian Group is dominated  
101 by psammite and metamorphosed semi-pelite deposited within a number of fault-bounded NE–  
102 SW-trending basins (Leslie et al. 2013). Analysis of detrital zircon, in which grains with  
103 Archaean ages are scarce, indicates derivation from Palaeo- and Mesoproterozoic (meta)granitic  
104 rocks (Cawood et al. 2003) that could have been sourced both from the west and/or east, as there  
105 is little difference in the protolith ages of the major crustal blocks that comprise east Laurentia  
106 and west Baltica (Banks et al. 2007; Kirkland et al. 2011). The Grampian Group is conformably  
107 overlain by the Appin Group, which consists of quartzite, psammite, metapelite and  
108 metacarbonate, the latter increasing towards the top. Parts of the Appin Group show remarkable  
109 stratigraphic continuity across the Grampian Terrane and may be traced laterally over several  
110 hundred kilometres. A Re–Os age of  $659.6 \pm 9.6$  Ma from a pyritiferous graphitic slate from the  
111 Ballachulish Slate Formation (mid Appin Group) is interpreted as the age of deposition (Rooney  
112 et al. 2011). Detrital zircon spectra from a single sample of interlayered psammite–semipelite,  
113 also from the Ballachullish Subgroup, show peaks in the Neoarchaean era (2800–2650 Ma) and  
114 late Palaeoproterozoic era (1950–1775) Ma with only a single zircon grain of Mesoproterozoic  
115 age (Cawood et al. 2003).

116         At the base of the overlying Argyll Group, the Port Askaig Tillite is probably correlative  
117 with the global Middle Cryogenian (Sturtian) glaciation (Brasier and Shields 2000; McCay et al.  
118 2006; Chew et al. 2009; Prave et al. 2009), and passes upwards into metamorphosed quartzite,

119 pelite and limestone. At its top, the Argyll Group is characterised by extensive metamorphosed  
120 volcanic rocks and subvolcanic sills that are interbedded with carbonate. U–Pb zircon ages of  
121  $595 \pm 4$  Ma (Halliday et al. 1989) and  $601 \pm 4$  Ma (Dempster et al. 2002) from volcanic rocks  
122 within the Tayvallich Volcanic Formation provide an age of deposition of the uppermost Argyll  
123 Group. Detrital zircon age data from Argyll Group rocks reveal a broad spread of dates from  
124 Archaean to Neoproterozoic in which pronounced age peaks are generally absent (Cawood et al.  
125 2003). The Southern Highland Group is a thick turbidite sequence volumetrically dominated by  
126 (metamorphosed) greywacke with shale, limestone and volcanic rocks. The detritus is mostly of  
127 Neoproterozoic or Mesoproterozoic age, of which the former become dominant towards  
128 stratigraphically higher levels (Cawood et al. 2003). In all Dalradian rocks there is a general  
129 scarcity of detrital ages in the range 2400–2000 Ma.

130         In general, sedimentation of the Dalradian Supergroup records a transition from relatively  
131 shallow continental shelf to deep water turbidite deposits, whose depositional environment is  
132 commonly ascribed to protracted episodic lithospheric stretching and rifting during breakout of  
133 Laurentia from Rodinia during birth of the Iapetus Ocean (Harris et al. 1978; Anderton 1982,  
134 1985, 1988; Soper and Anderton 1984; Soper 1994; Glover et al. 1995). The lower parts of the  
135 Dalradian succession represents deposition on a stable slowly subsiding continental shelf, which  
136 later broke up into numerous fault-bounded sedimentary basins contemporaneous with basic  
137 volcanism; palaeocurrent studies indicate a sedimentary source to the northwest (Anderton 1985;  
138 Stephenson et al. 2013a). The uppermost Dalradian strata, which are characterised by a major  
139 influx of feldspar, are dominated by deep-water turbidites reflecting widening of the newly-  
140 formed Iapetus Ocean. Mineralogical characteristics of the uppermost Dalradian sedimentary  
141 rocks have been used to suggest the detritus was derived from a continental landmass to the  
142 southeast (Harris et al. 1978), while others propose the emergence of granitoid basement  
143 following the stripping of cover rocks from a source area to the northwest, consistent with sparse

144 palaeocurrent data (Harris and Pitcher 1975; Harris et al. 1978; Plant et al. 1984; Anderton  
145 1985).

146         The Buchan Block in northeast Scotland forms a broad horseshoe-shaped outcrop pattern  
147 of Dalradian rocks that are generally right way up (Fig. 1). It is bounded to the west and south by  
148 major shear zones and exhibits some profound differences compared with the rest of the  
149 Grampian Terrane (Stephenson *et al.*, 2013b; Fig. 1a). These differences include the presence of  
150 large layered mafic–ultramafic intrusions (the North-east Grampian Basic Suite), numerous  
151 peraluminous granite bodies and metasedimentary migmatites from which the granites may have  
152 been derived (Johnson et al. 2003), and the widespread development of low-pressure (andalusite  
153 to sillimanite) Buchan-type regional metamorphism (Read 1952; Harte and Hudson 1978) rather  
154 than Barrovian (kyanite to sillimanite) metamorphism (Barrow 1893, 1912) that characterises  
155 Dalradian rocks outside of the Buchan Block. Although the Buchan Block has been regarded by  
156 some as an exotic terrane thrust into place during Grampian orogenesis (Sturt et al. 1977;  
157 Ramsay and Sturt 1978), it is now generally regarded as autochthonous (Johnson et al. 2001b,  
158 2015; Stephenson et al. 2013b). At lower stratigraphic levels, rocks comprising semipelites,  
159 graphitic metapelites and psammites with minor metalimestones and metavolcanic rocks, are  
160 generally ascribed to the Argyll Group, whilst at higher stratigraphic levels within the core of the  
161 Buchan Block, a thick sequence of metaturbidites belongs to the Southern Highland Group (Fig.  
162 2).

163

164

## 165 **ANALYTICAL METHODS**

166

### 167 **Sample selection, preparation and characterisation**

168

169 Data were collected from four metasedimentary rocks (from west to east, samples BB1, BB3,  
170 BB5 and BB6) collected from coastal exposures within the Buchan Block (Fig. 2). One sample  
171 (BB6) is from the Argyll Group, and assigned to the Crinan Subgroup (Goodman 1991;  
172 Stephenson et al. 2013b); the others are from the Southern Highland Group of which, based on a  
173 structural cross-section of the area (Stephenson and Gould 1995), the proximity of the samples to  
174 the Argyll Group–Southern Highland Group contact and the metamorphic grade of the rocks  
175 (which increases down stratigraphy), BB1 is stratigraphically lowest and BB3 stratigraphically  
176 highest. BB6 is a coarse-grained granulite facies metapelitic migmatite (Johnson et al. 2001a, b;  
177 Johnson et al. 2015); BB1 (amphibolite facies staurolite zone) and BB3 (greenschist facies  
178 biotite zone) are from massive psammite units interbedded with metapelite; BB5 (amphibolite  
179 facies andalusite zone) is a semipelite containing sparse Mn-rich garnet.

180 Detrital zircon grains were separated from approximately 1 kg of each sample using  
181 SelFrag high voltage pulse power fragmentation and heavy liquid separation at the Department  
182 of Applied Geology, Curtin University. Grains were hand picked and mounted in 25 mm  
183 diameter epoxy resin discs. The grain mounts were polished to approximately half grain  
184 thickness then cleaned and carbon coated for backscattered, secondary electron and  
185 cathodoluminescence (CL) imaging on a Tescan MIRA3 scanning electron microscope (SEM) at  
186 the Microscopy & Microanalysis Facility, John de Laeter Centre, Curtin University using a  
187 working distance of 15 mm and an accelerating voltage of 10 kV.

188

#### 189 **Laser ablation ICP–MS analysis: U–Pb dating and trace element determination**

190

191 LA–ICP–MS data were collected at the GeoHistory Facility in the John de Laeter Centre, Curtin  
192 University. Zircons were analysed using a single spot placed in the core of grains, the precise  
193 location of which was chosen to avoid thin overgrowths and/or inclusions based on the CL  
194 images. Grains were ablated using a Resonetics RESolution M–50A–LR, incorporating a



195 COMPEX 102 excimer laser. Following a 15–20 second period of background analysis, samples  
196 were spot ablated for 30 s at a 7 Hz repetition rate using a 33  $\mu\text{m}$  beam and laser energy of 1.7  
197  $\text{J}/\text{cm}^2$  at the sample surface. The sample cell was flushed with ultrahigh purity He (flow rate of  
198  $0.68 \text{ L min}^{-1}$ ) and  $\text{N}_2$  ( $2.8 \text{ mL min}^{-1}$ ). Isotopic intensities were measured using an Agilent 7700s  
199 quadrupole ICP–MS with high purity Ar as the plasma gas (flow rate  $0.98 \text{ L min}^{-1}$ ). Most  
200 elements were monitored for 0.01 seconds with the exception of  $^{88}\text{Sr}$  (0.02 s),  $^{139}\text{La}$  (0.04 s),  
201  $^{141}\text{Pr}$  (0.04 s),  $^{204}\text{Pb}$ ,  $^{206}\text{Pb}$ ,  $^{207}\text{Pb}$ ,  $^{208}\text{Pb}$  (all 0.03 s),  $^{232}\text{Th}$  (0.0125 s), and  $^{238}\text{U}$  (0.0125 s).  
202 International glass standard NIST 610 was used as the primary standard to calculate elemental  
203 concentrations (using  $^{29}\text{Si}$  as the internal standard element and assuming 14.76% Si in zircon)  
204 and to correct for instrument drift. For improved matrix matching,  $^{178}\text{Hf}$  in zircon was  
205 determined using GJ-1 (Jackson et al. 2004) with  $^{91}\text{Zr}$  as the internal standard element. Standard  
206 blocks were typically run after 20 unknown analyses. During the time-resolved analysis,  
207 contamination resulting from inclusions and compositional zoning were monitored and only the  
208 relevant part of the signal was integrated. The trace element results for NIST 612 (secondary  
209 standard) using NIST 610 as the reference material indicate that the accuracy was better than 2%  
210 for most elements. Only analyses with negligible common Pb were considered when placing age  
211 constraints.

212         The primary reference material used for U–Pb dating in this study was GJ-1 ( $601.7 \pm 1.4$   
213 Ma (Jackson et al. 2004; Kylander-Clark et al. 2013) with 91500 ( $1062.4 \pm 0.4$  Ma;  
214 (Wiedenbeck et al. 1995) and Plesovice ( $337.13 \pm 0.37$  Ma; (Sláma et al. 2008) used as  
215 secondary age standards.  $^{238}\text{U}/^{206}\text{Pb}$  ages calculated for all zircon age standards, treated as  
216 unknowns, were found to be within 3% of the accepted value. For example, the mean  $^{238}\text{U}/^{206}\text{Pb}$   
217 age determined for 91500 across all runs was  $1062 \pm 8$  Ma ( $2\sigma$ ,  $n = 24$ ,  $\text{MSWD} = 1.8$ ), consistent  
218 with the recommended values. The time-resolved mass spectra were reduced using the  
219 U\_Pb\_Geochronology3 and Trace Element data reduction schemes in Iolite (Paton et al. 2011)  
220 and references therein) and in-house excel macros. We consider those analyses within analytical

221 uncertainty ( $2\sigma$ ) of the concordia curve to be concordant. In cases where the true location of the  
222 mean data point can be assumed to fall on the concordia curve, it is possible to calculate a  
223 ‘concordia age’ (Ludwig, 1998), which makes best use of all  $^{207}\text{Pb}^*/^{206}\text{Pb}^*$  and  $^{238}\text{U}/^{206}\text{Pb}^*$  ratios.  
224 This approach typically yields a more precise mean age than by using either ratio alone, and also  
225 provides an objective and quantitative measure of concordance. The full data set is provided in  
226 Supplementary data Tables S1 (U–Pb) and S2 (trace elements).

227

228

## 229 **RESULTS**

230

### 231 **Zircon morphology**

232

233 Analysed zircon grains from samples BB1 and BB3 are mostly 100–200  $\mu\text{m}$  in the longest  
234 dimension and have low aspect ratios (2:1 or less). Those from BB5 and BB6 are smaller  
235 (mostly 50–100  $\mu\text{m}$ ) and contain a higher proportion of prismatic grains with aspect ratios up to  
236 5:1. In all samples, the majority of grains are rounded suggesting significant transport distances,  
237 although faceted grains are not uncommon.

238         The zircon grains exhibit diverse internal morphologies when imaged by CL. They range  
239 from simple broadly homogeneous grains to crystals with complex cores showing variable CL  
240 response that are commonly associated with one or more overgrowths (Fig. S1). Zircon cores  
241 commonly show fine oscillatory zoning typical of growth in a magmatic environment. In other  
242 cases cores exhibit sector or parallel zonation and/or irregular, diffuse patterns in CL response,  
243 the latter probably reflecting multiple phases of resorption and reprecipitation. Cores are  
244 commonly surrounded by overgrowths of broadly uniform and brighter CL response that are up  
245 to a few tens of microns in width, although overgrowths with CL responses darker than cores  
246 also occur. The overgrowths likely record zircon precipitation during some discrete (i.e. post-

247 magmatic) metamorphic, metasomatic or hydrothermal event. In many cases the overgrowths are  
248 sharply truncated, suggesting they may have developed prior to deposition of their sedimentary  
249 host rocks. However, some examples, particularly in the highest-grade migmatitic sample (BB6),  
250 are continuous and may record growth of new zircon during high-grade (Grampian)  
251 metamorphism of the sedimentary host rocks (Johnson et al. 2015).

252

### 253 **Detrital zircon age data**

254

255 The age data are discussed below in order of the inferred decreasing age of deposition of the  
256 metasedimentary protoliths (i.e. first BB6 then BB1, BB5 and BB3). Tera–Waserburg concordia  
257 diagrams for the four samples are shown in Fig. 3. Figure 4 shows frequency distribution  
258 diagrams, in which the grey filled area is the kernel density estimate for concordant data only  
259 and the dashed grey line is the kernel density estimate incorporating all data; the thin black line  
260 is the probability estimate for the concordant data only (Vermeesch 2012). All dates reported in  
261 the text are concordia ages with uncertainties quoted at the two-sigma level.

262           In the oldest sample (BB6) from the Argyll Group, 64 (73%) of 88 grains  
263 analysed were concordant (i.e. overlap the concordia curve within the  $2\sigma$  limit of uncertainty). In  
264 two of the three Southern Highland Group samples, the majority of analysed grains ages were  
265 concordant (in BB1 75% of 100 grains; in BB3 of 62% of 98 grains). However, for sample BB5,  
266 of 91 grains analysed only 32 (35%) were concordant (Fig. 3).

267           Of the concordant data from the Argyll Group sample (BB6), the vast majority lie within  
268 a more-or-less continuous spread of ages from the youngest grain at  $585 \pm 20$  Ma to c. 2000 Ma  
269 (Fig. 3a). Four grains have Neoproterozoic ages between c. 2500 and 2700 Ma, and a single grain  
270 has an age ( $3231 \pm 36$  Ma) close to the Neoproterozoic–Mesoproterozoic transition. Kernel density  
271 estimates for the data from sample BB6 indicate a prominent late Mesoproterozoic age peak at

272 1000–1100 Ma, with less well-defined peaks at around 1500 Ma and between 2500 and 3000 Ma  
273 (Fig. 4a).

274 Of the concordant data from sample BB1, most have ages between c. 900 and 2000 Ma,  
275 with the remaining data scattered to older ages, the oldest of which are around 3000 Ma (Fig.  
276 3b). Compared to BB6, kernel density estimates again show a dominant late Mesoproterozoic  
277 peak but a more pronounced Palaeoproterozoic peak at 1700–1800 Ma. The oldest data yields a  
278 much smaller broad peak of Archaean ages between 2500 and 3000 Ma (Fig. 4a).

279 Of the relatively few concordant data from sample BB5, there is a clear cluster of ages  
280 between 1700 and 2000 Ma and a smear of Neoarchaean ages; a few zircon cores have ages that  
281 are both younger and older (Fig. 3c). The youngest concordant age is  $948 \pm 30$  Ma, and the  
282 oldest is  $3008 \pm 16$  Ma. Kernel density estimates for sample BB5 yield two clear age peaks at  
283 around 1850 Ma and 2700 Ma (Fig. 4c). Much of the discordant data appears to define two broad  
284 trends, one extending from the concordant Archaean data towards younger ages, and another  
285 from the Palaeoproterozoic data towards younger ages. These trends are consistent with partial  
286 resetting of detrital zircon during Caledonian (*sensu lato*) tectonothermal events.

287 Similar to sample BB5, the concordant data from the youngest sample (BB3) show a  
288 tight cluster of ages at 1800–2000 Ma and a smear of older ages from around 2400 Ma to 3000  
289 Ma (Fig. 3d). A single grain with an Eoarchaean age of  $3654 \pm 18$  Ma is the oldest from all  
290 samples analysed. Most notably, there are no concordant data younger than Mesoproterozoic in  
291 this sample, with the youngest grain having an age of  $1786 \pm 30$  Ma. Kernel density estimates  
292 for sample BB3 again yield two clear age peaks, one at 1800–1900 Ma and a dominant Archaean  
293 peak at 2700–2800 Ma (Fig. 4d). In all samples there is a scarcity of concordant ages between c.  
294 2000 and 2400 Ma (Fig. 3 & 4).

295

296 **Trace element composition of zircon**

297

298 Considering only those grains yielding concordant U–Pb ages, the analysed trace element  
299 compositions of the detrital zircons show significant scatter and few clear trends with age (Fig.  
300 S2). Although the maximum concentration of Th in Archaean grains is smaller than in  
301 Proterozoic grains, there is no obvious difference in concentrations of U or in the U/Th ratio with  
302 age. All grains have typical steep chondrite-normalised (McDonough and Sun 1995) REE  
303 patterns although the absolute abundance of REE in individual grains varies by almost two  
304 orders of magnitude (Fig. 5a). Most grains, particularly those with low overall REE abundances,  
305 exhibit a negative Eu anomaly (Fig. 5a). In a plot of age vs  $\text{Eu}/\text{Eu}^*$ , Mesoproterozoic grains  
306 (dominant ages of c. 1000 Ma) show a more restricted range of  $(\text{Eu}/\text{Eu}^*)_{\text{N}}$  ( $<0.5$ ) compared with  
307 Palaeoproterozoic grains (~1800 Ma), with Archaean examples showing the highest measured  
308 values that in some cases exceeds 0.9 (Fig. 5b). The samples show a significant range in the  
309 relative enrichment of heavy REE, although in most cases there is a significant slope in the  
310 middle to HREE in which  $(\text{Gd}/\text{Yb})_{\text{N}}$  is below 0.1. However, a significantly larger range  
311  $[(\text{Gd}/\text{Yb})_{\text{N}}$  up to 0.57] is shown by Palaeoproterozoic grains compared to those with  
312 Mesoproterozoic and Archaean ages (Fig. 5c). The range in concentration of both Nb and Ta are  
313 significantly higher in Mesoproterozoic grains compared to older examples. There are little clear  
314 differences in concentrations of Sr or Sr/Y ratios with age. Considering the discordant data, a  
315 clear correlation between the degree of discordance, which is up to 77%, and the concentrations  
316 of many elements, in particular Sr, Fe, Th and LREE, suggests enhanced incorporation of non-  
317 formula elements in altered zircon or the presence of micro-inclusions of other phases (Nasdala  
318 et al. 2010).

319

320

## 321 **DISCUSSION**

322

### 323 **Concordant age data**

324  
325 *Detrital source areas*  
326  
327 The concordant detrital age data for samples from the Buchan Block yield spectra similar to  
328 those reported from upper Dalradian Supergroup rocks from the Central Highlands of Scotland  
329 (Cawood et al. 2003) and Shetland (Strachan et al. 2013), and from the overlying Highland  
330 Border Complex (Cawood et al. 2012a). Kernel density estimates yield three clear age peaks in  
331 the Neoproterozoic (c. 2800–2700 Ma), Palaeoproterozoic (c. 1900–1800 Ma) and late  
332 Mesoproterozoic (c. 1100–1000 Ma) eras that correspond to known tectonomagmatic events in  
333 both Laurentia and Baltica (Gower et al. 1990; Gower 1996; Rivers 1997; Bingen and Solli  
334 2009). However, based on sparse faunal (Fletcher and Rushton 2007) and palaeocurrent evidence  
335 (Anderton 1985; Stephenson et al. 2013a), the Dalradian Supergroup is generally regarded as  
336 having been derived from, and deposited on the southeastern margin of, Laurentia (Cawood et al.  
337 2003, 2007b; McAteer et al. 2010a,b; Strachan et al. 2013; Chew and Strachan 2014; Dewey et  
338 al. 2015). Sparse palaeocurrent data from the Buchan Block similarly indicates source areas to  
339 the north and west (Loudon 1963).

340         The data from the Argyll Group sample (BB6) are dominated by late Mesoproterozoic  
341 (Grenville) ages with a significant contribution from Palaeoproterozoic and early  
342 Mesoproterozoic ages, likely corresponding to detritus derived from the Ketilidian–Makkovik,  
343 Labradorian, Torngat, New Quebec, Nagssugtoqidian and Pinwarian orogenic belts (Hoffman  
344 1988; Gower 1996; Kerr et al. 1997; Rivers 1997; Wasteneys et al. 1997) (for paleogeographic  
345 reconstructions see fig. 2 of Cawood et al. 2003b and fig. 6 of Strachan et al., 2013).

346 Successively younger samples from the Southern Highland Group show a decrease in the  
347 proportion of late Mesoproterozoic material and an increase in both Palaeoproterozoic and  
348 Archaean aged detritus, consistent with the trend noted in other studies (Cawood et al. 2003,  
349 2007b; Strachan et al. 2013). Combined, these data are consistent with erosion of the late

350 Mesoproterozoic then Palaeoproterozoic orogens to expose Archaean basement rocks of the  
351 Superior and/or North Atlantic cratons, which may have been uplifted in the footwalls of rift  
352 faults due to the continued breakup of Rodinia and opening of Iapetus (Cawood et al. 2007b).

353 To statistically assess the similarity of the source rocks, we compare the concordant data  
354 from the Buchan Block with existing detrital zircon data from Dalradian and equivalent strata  
355 elsewhere (Cawood et al. 2003; Breeding et al. 2004; Banks et al. 2007; Chew et al. 2008;  
356 McAteer et al. 2010a,b; Strachan et al. 2013) [see Table S1]. This is achieved by means of a  
357 Kolmogorov–Smirnov (K–S) test, which is widely used to test the null hypothesis that two  
358 distributions come from the same population. To further visualise the results of this statistical  
359 test we apply multi-dimensional scaling of the D value in the K–S test, as discussed in  
360 Vermeesch (2013) and Spencer and Kirkland (2016). This approach creates a two-dimensional  
361 map of points that summarises the differences in the age population structure (Fig. 6). In this  
362 procedure samples that are similar plot together, while those that are dissimilar are widely  
363 spaced, while the distance from the centre reflects the increasing incorporation of a detrital  
364 component that may characterize a specific population grouping. It is important to note that the  
365 orientation of the axes in Fig. 6 is arbitrary.

366 The results show that the detrital age spectra from the two oldest samples (BB6 and BB1)  
367 are statistically indistinguishable (at the 95% confidence level), as are those from the two  
368 youngest samples (BB5 and BB3) (Fig. 6). In addition, the age data from each of the Buchan  
369 Block samples is indistinguishable from several other Dalradian rocks, including some from the  
370 older Grampian Group near the base of the Dalradian Supergroup (Fig. 6). Considering all data,  
371 two broad trends are evident (grey arrows on Fig. 6) that are subparallel to the lines joining  
372 similar Buchan Block samples. Based on the age spectra for these samples, the vector joining  
373 BB6 and BB1 represents an increase in Palaeoproterozoic relative to late Mesoarchaeon detritus,  
374 and the vector from BB5 to BB3 an increase in Archaean detritus. However, such simple  
375 relationships are not so clearly defined by data from Dalradian rocks elsewhere (Fig. 6).

376 Together, the concordant data suggest that Dalradian rocks in the Buchan Block were derived  
377 from similar source rocks to those exposed elsewhere in the Grampian Terrane, including rocks  
378 in Ireland and Shetland. These similarities strengthen the argument that the Buchan Block is  
379 autochthonous.

380

### 381 *Age of the Buchan Block samples*

382

383 The youngest concordant analysis is from the core of a grain within sample BB6, which yields a  
384 concordia age of  $585 \pm 20$  Ma. Although this grain does not display oscillatory zoning typical of  
385 magmatic zircon, comprising a fractured CL-bright core surrounded by a darker CL-dark region  
386 and a thin ( $<10 \mu\text{m}$ ) discontinuous CL-bright rim, it shows no depletion in HREE [ $(\text{Gd}/\text{Yb})_{\text{N}} =$   
387  $0.11$ ; Fig. 5a] and growth during high-grade metamorphism in the presence of garnet, which is  
388 characterised by flat middle to heavy REE patterns, is not supported (Rubatto and Hermann  
389 2007; Taylor et al. 2015). Although growth in some non-magmatic environment is possible, the  
390 size ( $\sim 80 \mu\text{m}$ ) and textural features of this grain suggests it grew prior to incorporation into the  
391 sedimentary precursor of this rock (i.e. it is not a fragment of a metamorphic rim). If so, and  
392 given that no radiogenic-Pb loss can be detected in the U–Pb systematics of the analysis, then  
393 this age suggests that deposition of part of the Crinan Subgroup occurred no more than 8 Ma  
394 before deposition of the uppermost Argyll Group sediments at  $601 \pm 4$  (Dempster et al. 2002).

395

### 396 **Discordant age data**

397

398 In order to better understand the most likely timing of radiogenic-Pb loss we model the  
399 discordant age data from sample BB5 using a variety of times of assumed Pb loss with the  
400 resultant population compared to concordant data using the K-S statistic following the approach  
401 discussed in Morris et al., (2015). The approach assumes that the discordant population is



402 derived from a similar geological province with similar zircon age spectra to the concordant  
403 zircon population. For any specified time of Pb loss, the discordant data in concordia space (Fig.  
404 3c) can be used to calculate an upper intercept that, for that specified time of Pb loss, defines a  
405 model age. The process is repeated for every possible time of radiogenic Pb loss to produce a  
406 range of upper-intercept (model) ages for the discordant population that can then be compared  
407 with the concordant population. In a simple situation in which only one episode of Pb loss  
408 occurred, the greatest similarity between the modelled discordant population and the concordant  
409 population will be represented by a single probability peak that reflects the most likely time of  
410 that Pb loss event. Where multiple episodes of Pb loss may have occurred, the resultant  
411 probability distribution of model and concordant ages may not yield a single probability peak.  
412 However, provided some grains were significantly influenced only by a single Pb loss event, the  
413 method can yield important information.

414         The results of the statistical modelling for sample BB5 are shown in Fig. 7. That the  
415 probability curve does not rise to single well-defined peak is interpreted to reflect the effect of at  
416 least two radiogenic Pb loss events, including recent Pb mobility that affected at least some of  
417 the discordant population (Fig. 7). Nevertheless, a distinct peak in the probability curve at c.  
418 470-450 Ma is consistent with at least some of the zircon having been significantly affected by  
419 Pb loss during this time period (Fig. 7). Ages of c. 470 Ma are consistent with regional  
420 metamorphism, ductile deformation and intrusion of voluminous gabbroic magmas in the  
421 Buchan Block (Dempster et al. 1995; Carty et al. 2012), and are broadly synchronous with  
422 Barrovian metamorphism elsewhere in the Grampian terrane (Oliver et al. 2000; Baxter et al.  
423 2002; Viète et al. 2013). Ages of 450 Ma broadly correspond to the youngest reported mica  
424  $^{40}\text{Ar}/^{39}\text{Ar}$  and Rb–Sr ages that date cooling of the Dalradian following the Grampian event  
425 (Dempster 1985; Dempster et al. 1995).

426

427 **Trace element compositions**

428

429 There are few clear trends between the age of concordant detrital zircon grains and the  
430 concentrations or ratios of analysed trace elements. The overall increase in  $\text{Eu}/\text{Eu}^*$  with age (Fig.  
431 5b) is difficult to interpret, but may reflect a systematic change in the abundance or composition  
432 of coexisting plagioclase and/or oxygen fugacity as magmatic zircon grew (Bédard 2006). The  
433 larger range of values of  $(\text{Gd}/\text{Yb})_N$  in Palaeoproterozoic grains compared to those with  
434 Mesoproterozoic and Archaean ages (Fig. 5c) might suggest more zircon equilibrated with  
435 garnet and a deeper origin for a greater proportion of the Palaeoproterozoic source rocks  
436 (Rubatto and Hermann 2007; Taylor et al. 2015). The lack of any clear trends in the bulk of the  
437 trace element data, and the large scatter in the data for which any trend that may exist, suggests  
438 the late Mesoproterozoic to Archaean source rocks were not significantly different.

439

440

## 441 CONCLUSIONS

442

- 443 • Concordant age spectra from Dalradian Supergroup sediments deposited in the fault-  
444 bounded Buchan Block were dominantly derived from late Mesoproterozoic and  
445 Palaeoproterozoic orogens and their Archaean basement rocks. The data are consistent  
446 with a Laurentian source;
- 447 • Archaean basement rocks (Superior and/or North Atlantic cratons) remained largely  
448 covered until deposition of the upper Dalradian rocks (Argyll and Southern Highland  
449 Groups)
- 450 • The source areas of sediments on the Buchan Block are not dissimilar to Dalradian rocks  
451 elsewhere – although the Buchan Block may conceivably have been translated significant  
452 distances into its current position during Grampian orogenesis, it is not exotic;

- 453       • Some detrital zircons were variably affected by Pb-loss at around 470–450 Ma,  
454       corresponding to Grampian orogenesis.
- 455       • Multidimensional scaling, REE content, and Pb-loss modelling are useful tools in  
456       maximizing the information extracted from detrital zircon datasets.

457

458

459   **ACKNOWLEDGEMENTS**

460

461   We are indebted to J. Dean for help with fieldwork and T. Jude-Eton for assistance with sample  
462   preparation. We thank M. Flowerdew & R. Strachan for their generous reviews and A. Carter for  
463   his expeditious editorial handling.

464 **Figure captions**

465  
466 **Fig. 1.** Regional map of the British Isles showing the location of the Grampian Terrane and  
467 major faults including the inferred position of the Iapetus suture. FHCBL = Fair Head–Clew Bay  
468 line. Modified after Neilson et al. (2009), Stephenson et al. (2013a) and Strachan et al. (2013).

469  
470 **Fig. 2.** Simplified geological map of the Buchan Block and surrounding rocks in the northeast  
471 Grampian Highlands of Scotland, showing the distribution of Dalradian Supergroup, intrusive  
472 rocks and the overlying Old Red Sandstone (Devonian) based on bedrock data from  
473 DiGMapGB-625, with the permission of the British Geological Survey. The position of the  
474 regional (D2) shear zones is from Ashcroft et al. (1984). The location of the four studied samples  
475 are indicated. The inset shows the location of the study area within Scotland.

476  
477 **Fig. 3.** Tera–Waserburg concordia diagrams for detrital zircons from the four analysed samples.  
478 Open circles are ages in Ma. The samples are arranged in inferred stratigraphic order. The oldest,  
479 sample, BB6, is from the Argyll Group (a); the others (b–d) are from the Southern Highland  
480 Group (SHG). Black symbols show concordant data that are within  $2\sigma$  error of the concordia;  
481 grey symbols are discordant.

482  
483 **Fig. 4.** Frequency–distribution diagrams of detrital zircon ages from the four analysed samples  
484 arranged in inferred stratigraphic order. The grey filled area is the kernel density estimate for  
485 concordant data (conc.) only; the dashed grey line is the kernel density estimate incorporating all  
486 data. The fine black line is the probability estimate for the concordant data only. The thin vertical  
487 lines demarcate boundaries between the Hadean (Had.), Archaean, Proterozoic and Phanerozoic  
488 (Phan.) eons; the Proterozoic is further subdivided into eras.

489

490 **Fig. 5.** Trace element data from zircon. (a) Chondrite-normalised REE plots of analysed zircon  
491 from the four samples (undifferentiated). The composition of the youngest grain (BB6-42) is  
492 indicated. Binary variation diagrams showing the chondrite-normalised (McDonough and Sun  
493 1995) ratio of: (b)  $\text{Eu}/\text{Eu}^*$ , and (c)  $\text{Gd}/\text{Yb}$ .

494  
495 **Fig. 6.** Non parametric multidimensional scaling plot of the detrital zircon age spectra from  
496 Dalradian Supergroup and related samples. The orientation of the diagram is arbitrary. Less  
497 dissimilar samples plot closer together. The thin lines join samples whose detrital zircon age data  
498 are statistically indistinguishable at the 95% confidence level. Sources of the U–Pb data: Banks  
499 et al. (2007), Cawood et al. (2003), Chew et al. (2008), McAteer et al. (2010a,b) and Strachan et  
500 al. (2013).

501

502 **Fig. 7.** Probability (P) of dissimilarity between discordant and concordant detrital zircon  
503 populations vs. time of radiogenic Pb loss.

504 **Supplementary information**

505

506 **Fig. S1.** Cathodoluminescence images of zircon from the four analysed samples.

507

508 **Fig. S2.** Selected chondrite-normalised trace element plots.

509

510 **Table S1.** U–Pb age data (LA–ICPMS).

511

512 **Table S2.** Chondrite normalised trace element data (LA–ICPMS).

513

514 **Table S3.** Matrix showing results of Kolmogorov–Smirnov (K–S) test comparing the Buchan  
515 Block samples of the current study with other Dalradian and related samples. The hypothesis that  
516 two samples come from the same source is rejected when the probability ( $p$ ) drops below 0.05,  
517 indicating that we have 95% confidence that the samples are different. Those samples whose  
518 detrital zircon age data are statistically indistinguishable at the 95% confidence level are  
519 highlighted in yellow.

520

521

522

523

524

525 **REFERENCES**

- 526
- 527 Andersen, T. 2005. Detrital zircons as tracers of sedimentary provenance: limiting  
528 conditions from statistics and numerical simulation. *Chemical Geology*, **216**, 249–270.
- 529 Anderton, R. 1982. Dalradian deposition and the late Precambrian-Cambrian history of the  
530 N Atlantic region: A review of the early evolution of the Iapetus Ocean. *Journal of the*  
531 *Geological Society*, **139**, 21–431, <http://dx.doi/10.1144/gsjgs.139.4.0421>.
- 532 Anderton, R. 1985. Sedimentation and tectonics in the Scottish Dalradian. *Scottish Journal*  
533 *of Geology*, **21**, 407–436.
- 534 Anderton, R. 1988. Dalradian slides and basin development: a radical interpretation of  
535 stratigraphy and structure in the SW and Central Highlands of Scotland. *Journal -*  
536 *Geological Society (London)*, **145**, 669–678.
- 537 Banks, C.J., Smith, M., Winchester, J.A., Horstwood, M.S.A., Noble, S.R. & Ottley, C.J. 2007.  
538 Provenance of intra-Rodinian basin-fills: The lower Dalradian Supergroup, Scotland.  
539 *Precambrian Research*, **153**, 46–64, <http://dx.doi/10.1016/j.precamres.2006.11.004>.
- 540 Barrow, G. 1893. On an Intrusion of Muscovite-biotite Gneiss in the South-eastern  
541 Highlands of Scotland, and its accompanying Metamorphism. *Quarterly Journal of the*  
542 *Geological Society of London*, **49**, 330–358,  
543 <http://dx.doi/10.1144/GSL.JGS.1893.049.01-04.52>.
- 544 Barrow, G. 1912. On the geology of Lower Dee-side and the southern Highland Border.  
545 *Proceedings of the Geologists' Association*, **23**, 274–IN271.
- 546 Baxter, E.F., Ague, J.J. & Depaolo, D.J. 2002. Prograde temperature-time evolution in the  
547 Barrovian type-locality constrained by Sm/Nd garnet ages from Glen Clova, Scotland.  
548 *Journal of the Geological Society*, **159**, 71–82.
- 549 Bédard, J.H. 2006. Trace element partitioning in plagioclase feldspar. *Geochimica et*  
550 *Cosmochimica Acta*, **70**, 3717–3742, <http://dx.doi/10.1016/j.gca.2006.05.003>.

551 Bingen, B. & Solli, A. 2009. Geochronology of magmatism in the Caledonian and  
552 Sveconorwegian belts of Baltica: synopsis for detrital zircon provenance studies.  
553 *Norwegian Journal of Geology*, **89**, 267–290.

554 Brasier, M.D. & Shields, G. 2000. Neoproterozoic chemostratigraphy and correlation of the  
555 Port Askaig glaciation, Dalradian Supergroup of Scotland. *Journal of the Geological*  
556 *Society*, **157**, 909–914.

557 Breeding, C.M., Ague, J.J., Grove, M. & Rupke, A.L. 2004. Isotopic and chemical alteration of  
558 zircon by metamorphic fluids: U-Pb age depth-profiling of zircon crystals from  
559 Barrow's garnet zone, northeast Scotland. *American Mineralogist*, **89**, 1067–1077.

560 Carty, J.P., Connelly, J.N., Hudson, N.F.C. & Gale, J.F.W. 2012. Constraints on the timing of  
561 deformation, magmatism and metamorphism in the dalradian of NE Scotland. *Scottish*  
562 *Journal of Geology*, **48**, 103–117, <http://dx.doi/10.1144/sjg2012-407>.

563 Cawood, P., Merle, R., Strachan, R. & Tanner, P. 2012a. Provenance of the Highland Border  
564 Complex: constraints on Laurentian margin accretion in the Scottish Caledonides.  
565 *Journal of the Geological Society*, **169**, 575–586.

566 Cawood, P.A., Hawkesworth, C. & Dhuime, B. 2012b. Detrital zircon record and tectonic  
567 setting. *Geology*, **40**, 875–878.

568 Cawood, P.A., Hawkesworth, C.J. & Dhuime, B. 2013. The continental record and the  
569 generation of continental crust. *Bulletin of the Geological Society of America*, **125**, 14–  
570 32.

571 Cawood, P.A., Nemchin, A.A., Smith, M. & Loewy, S. 2003. Source of the Dalradian  
572 Supergroup constrained by U-Pb dating of detrital zircon and implications for the  
573 East Laurentian margin. *Journal of the Geological Society*, **160**, 231–246,  
574 <http://dx.doi/10.1144/0016-764902-039>.



- 575 Cawood, P.A., Nemchin, A.A. & Strachan, R. 2007a. Provenance record of Laurentian  
576 passive-margin strata in the northern Caledonides: Implications for paleodrainage  
577 and paleogeography. *Geological Society of America Bulletin*, **119**, 993–1003.
- 578 Cawood, P.A., Nemchin, A.A., Strachan, R., Prave, T. & Krabbendam, M. 2007b. Sedimentary  
579 basin and detrital zircon record along East Laurentia and Baltica during assembly and  
580 breakup of Rodinia. *Journal of the Geological Society*, **164**, 257–275.
- 581 Chew, D.M., Daly, J.S., Magna, T., Page, L.M., Kirkland, C.L., Whitehouse, M.J. & Lam, R. 2010.  
582 Timing of ophiolite obduction in the Grampian orogen. *Bulletin of the Geological*  
583 *Society of America*, **122**, 1787–1799.
- 584 Chew, D.M., Fallon, N., Kennelly, C., Crowley, Q. & Pointon, M. 2009. Basic volcanism  
585 contemporaneous with the Sturtian glacial episode in NE Scotland. *Transactions of the*  
586 *Royal Society of Edinburgh*, **100**, 399–415,  
587 <http://dx.doi/10.1017/S1755691009009037>.
- 588 Chew, D.M., Flowerdew, M.J., Page, L.M., Crowley, Q.G., Daly, J.S., Cooper, M. & Whitehouse,  
589 M.J. 2008. The tectonothermal evolution and provenance of the Tyrone Central Inlier,  
590 Ireland: Grampian imbrication of an outboard Laurentian microcontinent? *Journal of*  
591 *the Geological Society*, **165**, 675–685, <http://dx.doi/10.1144/0016-76492007-120>.
- 592 Chew, D.M. & Strachan, R.A. 2014. The Laurentian Caledonides of Scotland and Ireland.  
593 *Geological Society, London, Special Publications*, **390**, 45–91.
- 594 Dempster, T.J. 1985. Uplift patterns and orogenic evolution in the Scottish Dalradian.  
595 *Journal of the Geological Society*, **142**, 111–128.
- 596 Dempster, T.J., Hudson, N.F.C. & Rogers, G. 1995. Metamorphism and cooling of the NE  
597 Dalradian. *Journal - Geological Society (London)*, **152**, 383–390.
- 598 Dempster, T.J., Rogers, G., Tanner, P.W.G., Bluck, B.J., Muir, R.J., Redwood, S.D., Ireland, T.R.  
599 & Paterson, B.A. 2002. Timing of deposition, orogenesis and glaciation within the

600 Dalradian rocks of Scotland: Constraints from U-Pb zircon ages. *Journal of the*  
601 *Geological Society*, **159**, 83–94, <http://dx.doi/10.1144/0016-764901061>.

602 Dewey, J. & Mange, M. 1999. Petrography of Ordovician and Silurian sediments in the  
603 western Irish Caledonides: tracers of a short-lived Ordovician continent-arc collision  
604 orogeny and the evolution of the Laurentian Appalachian-Caledonian margin.  
605 *Geological Society, London, Special Publications*, **164**, 55–107.

606 Dewey, J.F., Dalziel, I.W., Reavy, R.J. & Strachan, R.A. 2015. The Neoproterozoic to Mid-  
607 Devonian evolution of Scotland: a review and unresolved issues. *Scottish Journal of*  
608 *Geology*, **51**, 5–30.

609 Fletcher, T.P. & Rushton, A.W. 2007. The Cambrian fauna of the Leny Limestone, Perthshire,  
610 Scotland. *Earth and Environmental Science Transactions of the Royal Society of*  
611 *Edinburgh*, **98**, 199–218.

612 Glover, B., Key, R., May, F., Clark, G., Phillips, E. & Chacksfield, B. 1995. A Neoproterozoic  
613 multi-phase rift sequence: the Grampian and Appin groups of the southwestern  
614 Monadhliath Mountains of Scotland. *Journal of the Geological Society*, **152**, 391–406.

615 Goodman, S. 1991. The Pannanich Hill Complex and the origin of Crinan Subgroup  
616 migmatites in the north-eastern and central Highlands. *Scottish Journal of Geology*, **27**,  
617 147–156.

618 Gower, C., Ryan, A. & Rivers, T. 1990. Mid-Proterozoic Laurentia-Baltica: an overview of its  
619 geological evolution and a summary of the contributions made by this volume. *Mid-*  
620 *Proterozoic Laurentia-Baltica*, **38**, 1–20.

621 Gower, C.F. 1996. The evolution of the Grenville Province in eastern Labrador, Canada.  
622 *Geological Society, London, Special Publications*, **112**, 197–218.

623 Halliday, A., Graham, C., Aftalion, M. & Dymoke, P. 1989. Short Paper: The depositional age  
624 of the Dalradian Supergroup: U-Pb and Sm-Nd isotopic studies of the Tayvallich  
625 Volcanics, Scotland. *Journal of the Geological Society*, **146**, 3–6.

- 626 Harris, A., Baldwin, C., Bradbury, H., Johnson, H. & Smith, R. 1978. Ensialic basin  
627 sedimentation: the Dalradian Supergroup. *Crustal evolution in northwestern Britain  
628 and adjacent regions. Geological Journal Special*, **10**, 115–138.
- 629 Harris, A. & Pitcher, W. 1975. The Dalradian Supergroup. *A Correlation of the Precambrian  
630 Rocks of the British Isles. Geological Society, London, Special Reports*, **6**, 52–75.
- 631 Harris, A.L. 1994. The Dalradian Supergroup in Scotland, Shetland and Ireland. *A revised  
632 correlation of Precambrian rocks in the British Isles*, 33–53.
- 633 Harte, B. & Hudson, N.F.C. 1978. Pelite facies series and the temperatures and pressures of  
634 Dalradian metamorphism in E Scotland. *Geological Society Special Publication*, 323–  
635 337.
- 636 Hoffman, P.F. 1988. United Plates of America, the birth of a craton-Early Proterozoic  
637 assembly and growth of Laurentia. *Annual review of Earth and Planetary Sciences*, **16**,  
638 543–603.
- 639 Hoffman, P.F. & Schrag, D.P. 2002. The snowball Earth hypothesis: testing the limits of  
640 global change. *Terra Nova*, **14**, 129–155.
- 641 Jackson, S.E., Pearson, N.J., Griffin, W.L. & Belousova, E.A. 2004. The application of laser  
642 ablation-inductively coupled plasma-mass spectrometry to in situ U-Pb zircon  
643 geochronology. *Chemical Geology*, **211**, 47–69.
- 644 Johnson, T., Kirkland, C., Reddy, S. & Fischer, S. 2015. Grampian migmatites in the Buchan  
645 Block, NE Scotland. *Journal of Metamorphic Geology*, **33**, 695–709.
- 646 Johnson, T.E., Hudson, N.F.C. & Droop, G.T.R. 2001a. Melt segregation structures within the  
647 Inzie head gneisses of the Northeastern Dalradian. *Scottish Journal of Geology*, **37**, 59–  
648 72, <http://dx.doi/10.1144/sjg37020059>.
- 649 Johnson, T.E., Hudson, N.F.C. & Droop, G.T.R. 2001b. Partial melting in the Inzie Head  
650 gneisses: The role of water and a petrogenetic grid in KFMASH applicable to anatexis

651 pelitic migmatites. *Journal of Metamorphic Geology*, **19**, 99–118,  
652 <http://dx.doi/10.1046/j.0263-4929.2000.00292.x>.

653 Johnson, T.E., Hudson, N.F.C. & Droop, G.T.R. 2003. Evidence for a genetic granite-migmatite  
654 link of the Dalradian of NE Scotland. *Journal of the Geological Society*, **160**, 447–457.

655 Kerr, A., Hall, J., Wardle, R.J., Gower, C.F. & Ryan, B. 1997. New reflections on the structure  
656 and evolution of the Makkovikian - Ketilidian Orogen in Labrador and southern  
657 Greenland. *Tectonics*, **16**, 942–965.

658 Kirkland, C.L., Alsop, G.I., Daly, J.S., Whitehouse, M.J., Lam, R. & Clark, C. 2013. Constraints  
659 on the timing of Scandian deformation and the nature of a buried Grampian terrane  
660 under the Caledonides of northwestern Ireland. *Journal of the Geological Society*, **170**,  
661 615–625.

662 Kirkland, C.L., Bingen, B., Whitehouse, M.J., Beyer, E. & Griffin, W.L. 2011. Neoproterozoic  
663 palaeogeography in the North Atlantic Region: Inferences from the Akkajaure and  
664 Seve Nappes of the Scandinavian Caledonides. *Precambrian Research*, **186**, 127–146.

665 Košler, J., Fonneland, H., Sylvester, P., Tubrett, M. & Pedersen, R.-B. 2002. U–Pb dating of  
666 detrital zircons for sediment provenance studies—a comparison of laser ablation  
667 ICPMS and SIMS techniques. *Chemical Geology*, **182**, 605–618.

668 Kylander-Clark, A.R., Hacker, B.R. & Cottle, J.M. 2013. Laser-ablation split-stream ICP  
669 petrochronology. *Chemical Geology*, **345**, 99–112.

670 Leslie, A.G., Robertson, S., Smith, M., Banks, C.J., Mendum, J.R. & Stephenson, D. 2013. The  
671 Dalradian rocks of the northern Grampian Highlands of Scotland. *Proceedings of the  
672 Geologists' Association*, **124**, 263–317, <http://dx.doi/10.1016/j.pgeola.2012.07.010>.

673 Loudon, T.V., 1963. The sedimentation and structure in the Macduff District of North  
674 Banffshire and Aberdeenshire. Unpublished PhD Thesis. University of Edinburgh.

675 McAteer, C.A., Daly, J.S., Flowerdew, M.J., Connelly, J.N., Housh, T.B. & Whitehouse, M.J.  
676 2010a. Detrital zircon, detrital titanite and igneous clast U–Pb geochronology and

677 basement–cover relationships of the Colonsay Group, SW Scotland: Laurentian  
678 provenance and correlation with the Neoproterozoic Dalradian Supergroup.  
679 *Precambrian Research*, **181**, 21–42, <http://dx.doi/10.1016/j.precamres.2010.05.013>.

680 McAteer, C.A., Daly, J.S., Flowerdew, M.J., Whitehouse, M.J. & Kirkland, C.L. 2010b. A  
681 Laurentian provenance for the Dalradian rocks of north Mayo, Ireland, and evidence  
682 for an original basement-cover contact with the underlying Annagh Gneiss Complex.  
683 *Journal of the Geological Society*, **167**, 1033–1048.

684 McCay, G.A., Prave, A.R., Alsop, G.I. & Fallick, A.E. 2006. Glacial trinity: Neoproterozoic earth  
685 history within the British-Irish caledonides. *Geology*, **34**, 909–912,  
686 <http://dx.doi/10.1130/G22694A.1>.

687 McDonough, W.F. & Sun, S.-S. 1995. The composition of the Earth. *Chemical Geology*, **120**,  
688 223–253.

689 McKerrow, W., Mac Niocaill, C. & Dewey, J. 2000. The Caledonian orogeny redefined. *Journal*  
690 *of the Geological Society*, **157**, 1149–1154.

691 Morris, G.A., Kirkland, C.L., Pease, V. 2015. Orogenic paleofluid flow recorded by discordant  
692 detrital zircons in the Caledonian foreland basin of northern Greenland. *Lithosphere*,  
693 **7**, 138–143.

694 Nasdala, L., Hanchar, J.M., Rhede, D., Kennedy, A.K. & Váczi, T. 2010. Retention of uranium  
695 in complexly altered zircon: an example from Bancroft, Ontario. *Chemical Geology*,  
696 **269**, 290–300.

697 Neilson, J., Kokelaar, B. & Crowley, Q. 2009. Timing, relations and cause of plutonic and  
698 volcanic activity of the Siluro-Devonian post-collision magmatic episode in the  
699 Grampian Terrane, Scotland. *Journal of the Geological Society*, **166**, 545–561.

700 Oliver, G.J.H., Chen, F., Buchwaldt, R. & Hegner, E. 2000. Fast tectonometamorphism and  
701 exhumation in the type area of the Barrovian and Buchan zones. *Geology*, **28**, 459–  
702 462, [http://dx.doi/10.1130/0091-7613\(2000\)28<459:FTAET>2.0.CO](http://dx.doi/10.1130/0091-7613(2000)28<459:FTAET>2.0.CO).

703 Paton, C., Hellstrom, J., Paul, B., Woodhead, J. & Hergt, J. 2011. Iolite: Freeware for the  
704 visualisation and processing of mass spectrometric data. *Journal of Analytical Atomic*  
705 *Spectrometry*, **26**, 2508–2518.

706 Plant, J.A., Watson, J.V. & Green, P. 1984. Moine-Dalradian relationships and their  
707 palaeotectonic significance. *Proceedings of the Royal Society of London A:*  
708 *Mathematical, Physical and Engineering Sciences*. The Royal Society, 185–202.

709 Prave, A.R., Fallick, A.E., Thomas, C.W. & Graham, C.M. 2009. A composite C-isotope profile  
710 for the Neoproterozoic Dalradian Supergroup of Scotland and Ireland. *Journal of the*  
711 *Geological Society*, **166**, 845–857, <http://dx.doi/10.1144/0016-76492008-131>.

712 Ramsay, D.M. & Sturt, B.A. 1978. The status of the Banff nappe. *Geological Society Special*  
713 *Publication*, 145–151.

714 Read, H.H. 1952. Metamorphism and migmatization in the Ythan Valley, Aberdeenshire.  
715 *Transactions of the Edinburgh Geological Society*, **15**, 265–279.

716 Rivers, T. 1997. Lithotectonic elements of the Grenville Province: review and tectonic  
717 implications. *Precambrian Research*, **86**, 117–154.

718 Rooney, A.D., Chew, D.M. & Selby, D. 2011. Re-Os geochronology of the Neoproterozoic-  
719 Cambrian Dalradian Supergroup of Scotland and Ireland: Implications for  
720 Neoproterozoic stratigraphy, glaciations and Re-Os systematics. *Precambrian*  
721 *Research*, **185**, 202–214, <http://dx.doi/10.1016/j.precamres.2011.01.009>.

722 Rubatto, D. & Hermann, J. 2007. Experimental zircon/melt and zircon/garnet trace element  
723 partitioning and implications for the geochronology of crustal rocks. *Chemical*  
724 *Geology*, **241**, 38–61.

725 Sláma, J., Košler, J., Condon, D.J., Crowley, J.L., Gerdes, A., Hanchar, J.M., Horstwood, M.S.,  
726 Morris, G.A., Nasdala, L. & Norberg, N. 2008. Plešovice zircon—a new natural  
727 reference material for U–Pb and Hf isotopic microanalysis. *Chemical Geology*, **249**, 1–  
728 35.

729 Soper, N.J. 1994. Was Scotland a Vendian RRR junction? *Journal - Geological Society*  
730 *(London)*, **151**, 579–582.

731 Soper, N.J. & Anderton, R. 1984. Did the Dalradian slides originate as extensional faults?  
732 *Nature*, **307**, 357–360, <http://dx.doi/10.1038/307357a0>.

733 Spencer, C.J. & Kirkland, C.L. 2015. Visualizing the sedimentary response through the  
734 orogenic cycle: A multidimensional scaling approach. *Lithosphere*, L479. 471.

735 Spencer, C.J. & Kirkland, C.L. 2016. Visualizing the sedimentary response through the  
736 orogenic cycle: A multidimensional scaling approach. *Lithosphere*, **8**, 29–37.

737 Stephenson, D. & Gould, D.E. 1995. The Grampian Highlands. Bernan Assoc.

738 Stephenson, D., Mendum, J.R., Fettes, D.J. & Leslie, A.G. 2013a. The Dalradian rocks of  
739 Scotland: An introduction. *Proceedings of the Geologists' Association*, **124**, 3–82.

740 Stephenson, D., Mendum, J.R., Fettes, D.J., Smith, C.G., Gould, D., Tanner, P.W.G. & Smith, R.A.  
741 2013b. The Dalradian rocks of the north-east Grampian Highlands of Scotland.  
742 *Proceedings of the Geologists' Association*, **124**, 318–392.

743 Strachan, R., Prave, A., Kirkland, C. & Storey, C. 2013. U–Pb detrital zircon geochronology of  
744 the Dalradian Supergroup, Shetland Islands, Scotland: implications for regional  
745 correlations and Neoproterozoic–Palaeozoic basin development. *Journal of the*  
746 *Geological Society*, **170**, 905–916.

747 Sturt, B.A., Ramsay, D.M., Pringle, I.R. & Tegg, D.E. 1977. Precambrian gneisses in the  
748 Dalradian sequence of northeast Scotland. *Journal of the Geological Society*, **134**, 41–  
749 44, <http://dx.doi/10.1144/gsjgs.134.1.0041>.

750 Tanner, P.W.G. 2014. A kinematic model for the Grampian Orogeny, Scotland. *Geological*  
751 *Society Special Publication*, 467–511.

752 Tanner, P.W.G. & Pringle, M.S. 1999. Testing for the presence of a terrane boundary within  
753 Neoproterozoic (Dalradian) to Cambrian siliceous turbidites at Callander, Perthshire,

754 Scotland. *Journal of the Geological Society*, **156**, 1205–1216,  
755 <http://dx.doi/10.1144/gsjgs.156.6.1205>.

756 Tanner, P.W.G. & Sutherland, S. 2007. The Highland Border Complex, Scotland: A paradox  
757 resolved. *Journal of the Geological Society*, **164**, 111–116,  
758 <http://dx.doi/10.1144/0016-76492005-188>.

759 Taylor, R., Harley, S., Hinton, R., Elphick, S., Clark, C. & Kelly, N. 2015. Experimental  
760 determination of REE partition coefficients between zircon, garnet and melt: a key to  
761 understanding high - T crustal processes. *Journal of Metamorphic Geology*, **33**, 231–  
762 248.

763 Vermeesch, P. 2012. On the visualisation of detrital age distributions. *Chemical Geology*,  
764 **312**, 190–194.

765 Vermeesch, P. 2013. Multi-sample comparison of detrital age distributions. *Chemical*  
766 *Geology*, **341**, 140–146.

767 Viete, D.R., Oliver, G.J.H., Fraser, G.L., Forster, M.A. & Lister, G.S. 2013. Timing and heat  
768 sources for the Barrovian metamorphism, Scotland. *Lithos*, **177**, 148–163.

769 Wasteneys, H., Kamo, S., Moser, D., Krogh, T., Gower, C. & Owen, J. 1997. U–Pb  
770 geochronological constraints on the geological evolution of the Pinware terrane and  
771 adjacent areas, Grenville Province, southeast Labrador, Canada. *Precambrian*  
772 *Research*, **81**, 101–128.

773 Wiedenbeck, M., Alle, P., Corfu, F., Griffin, W., Meier, M., Oberli, F., Quadt, A.v., Roddick, J. &  
774 Spiegel, W. 1995. Three natural zircon standards for U - Th - Pb, Lu - Hf, trace  
775 element and REE analyses. *Geostandards Newsletter*, **19**, 1–23.

776  
777



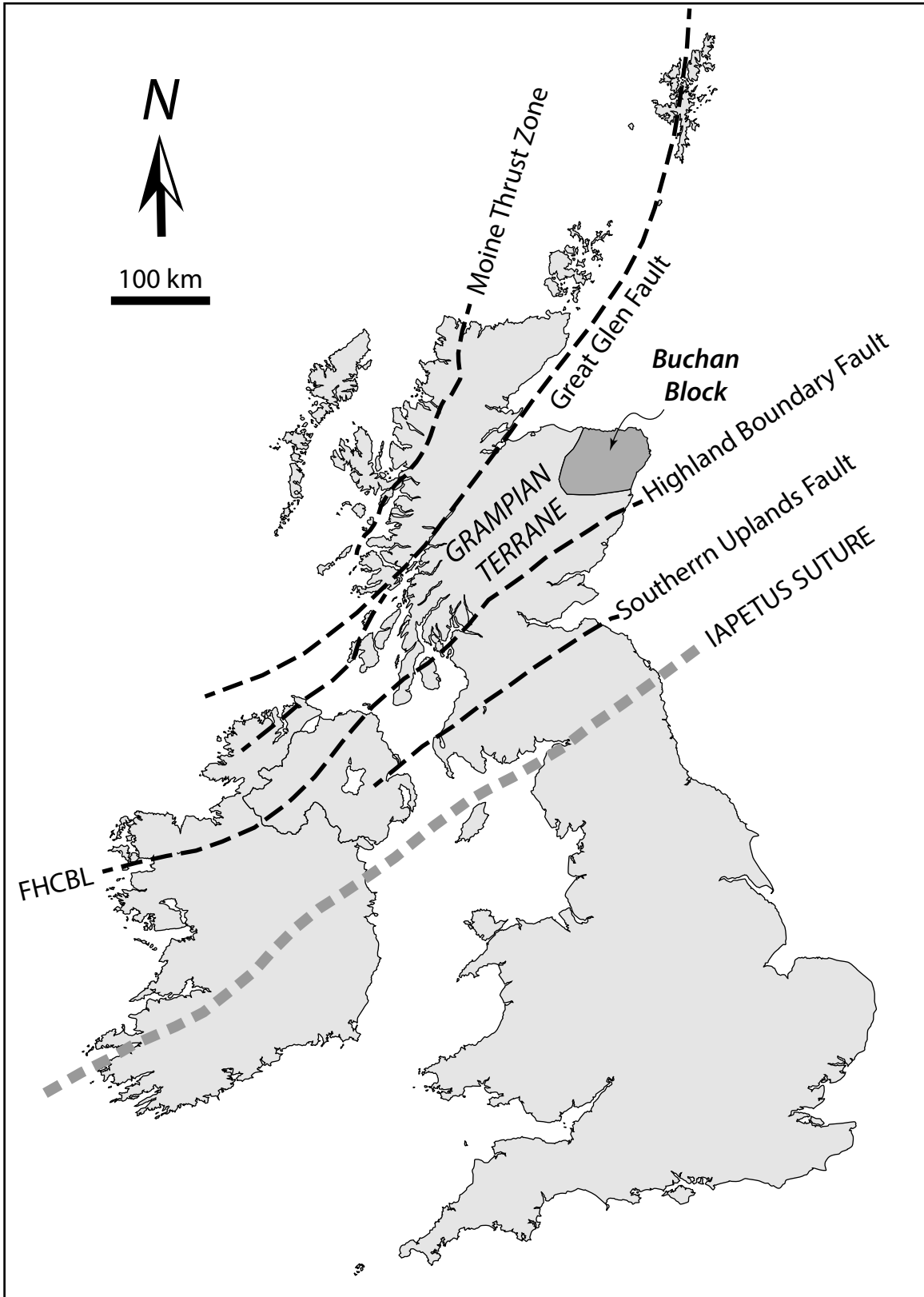


Figure 1

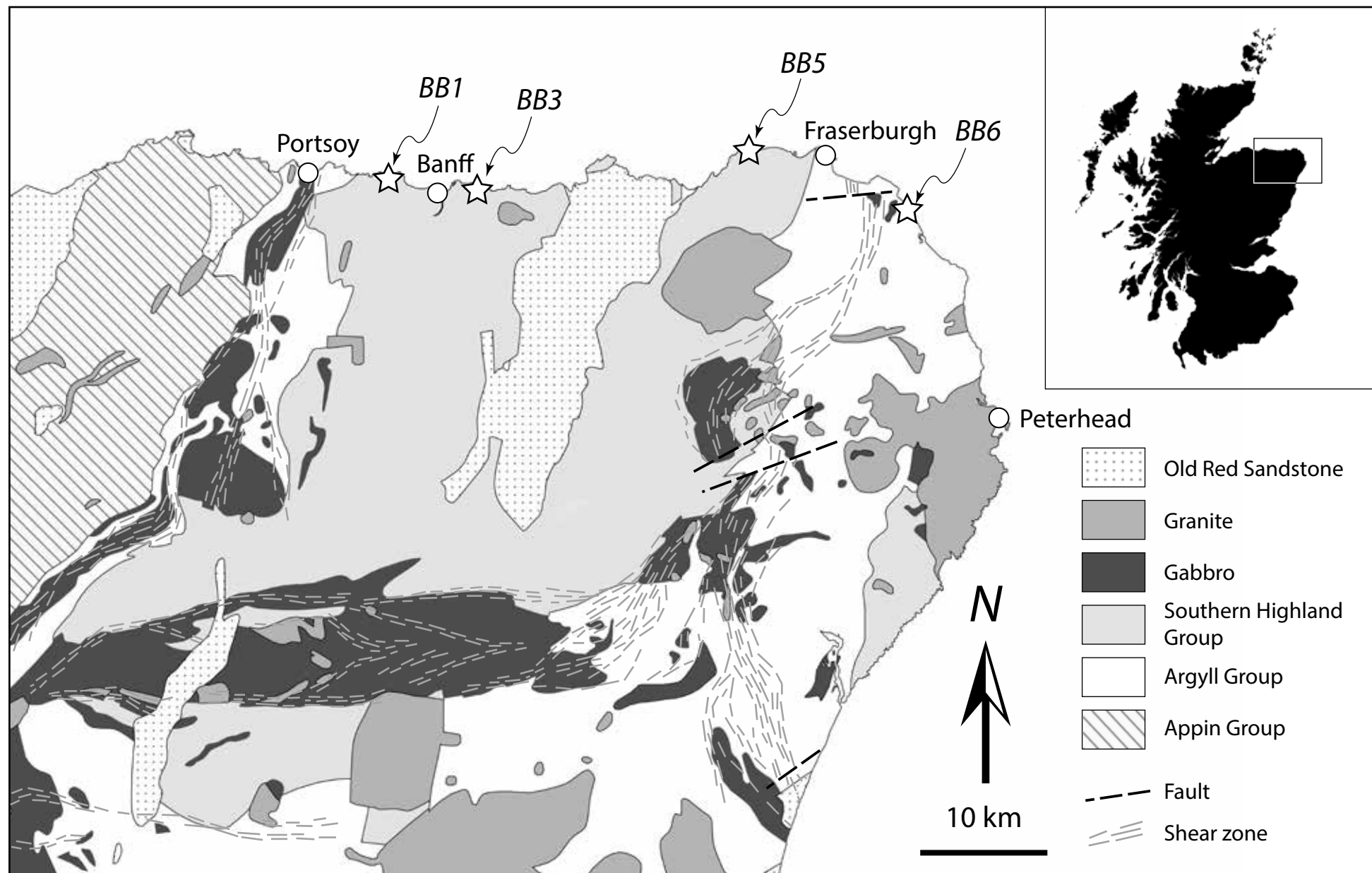


Figure 2

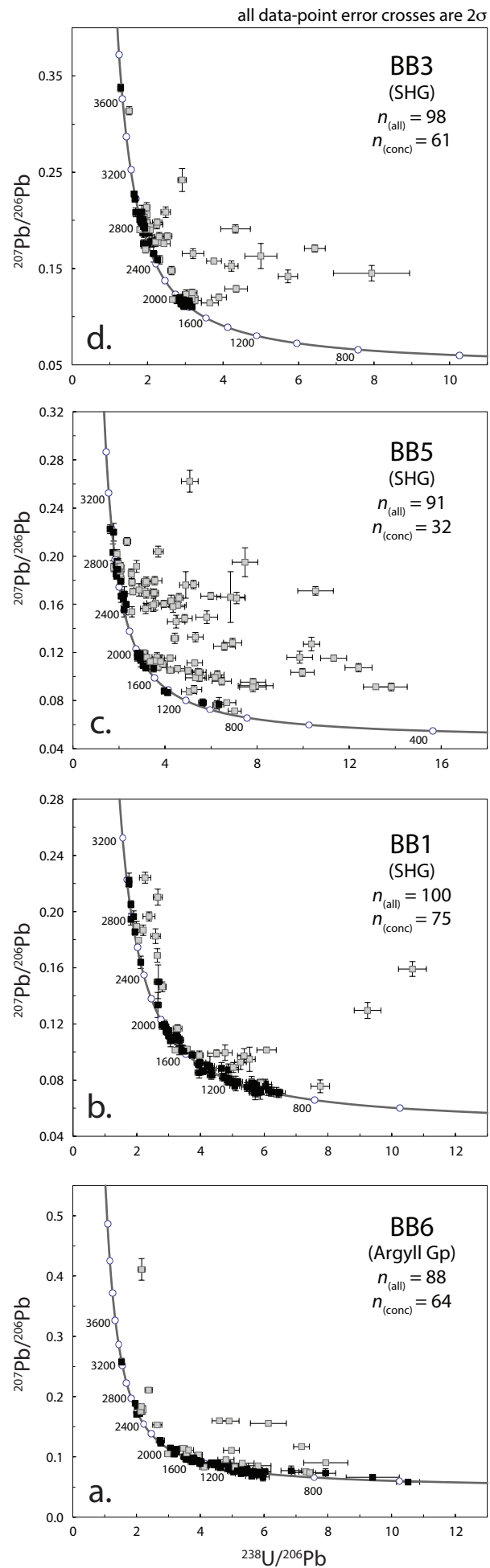


Figure 3

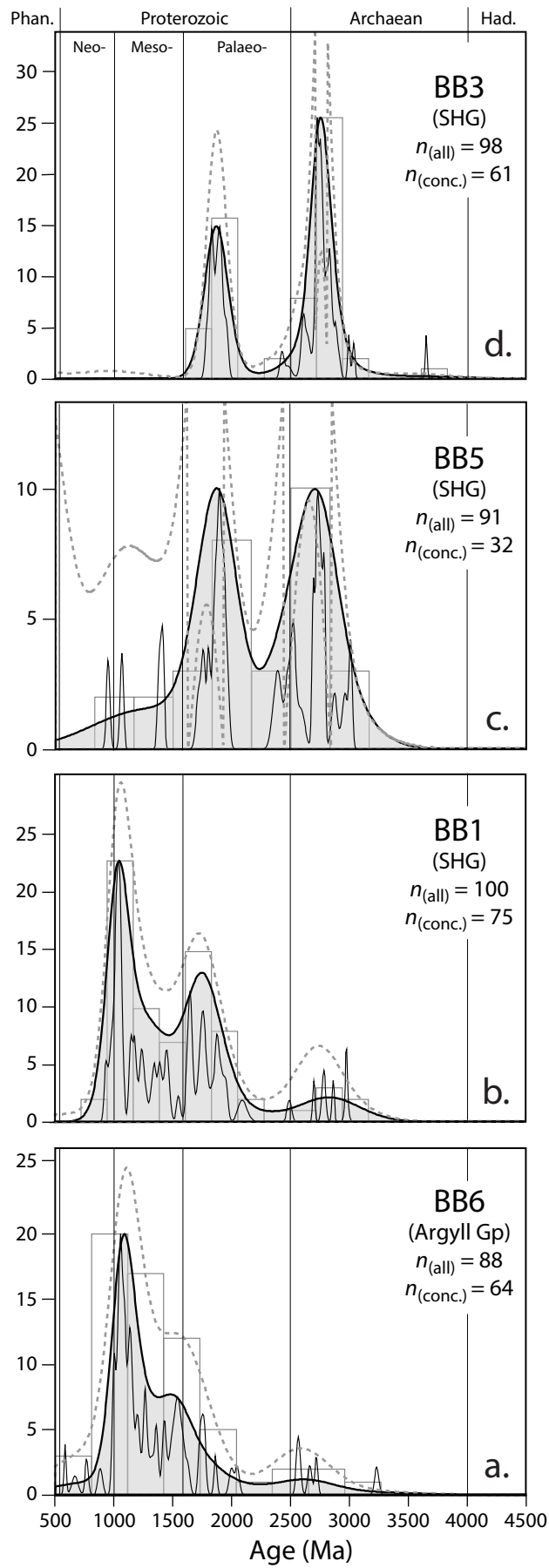


Figure 4

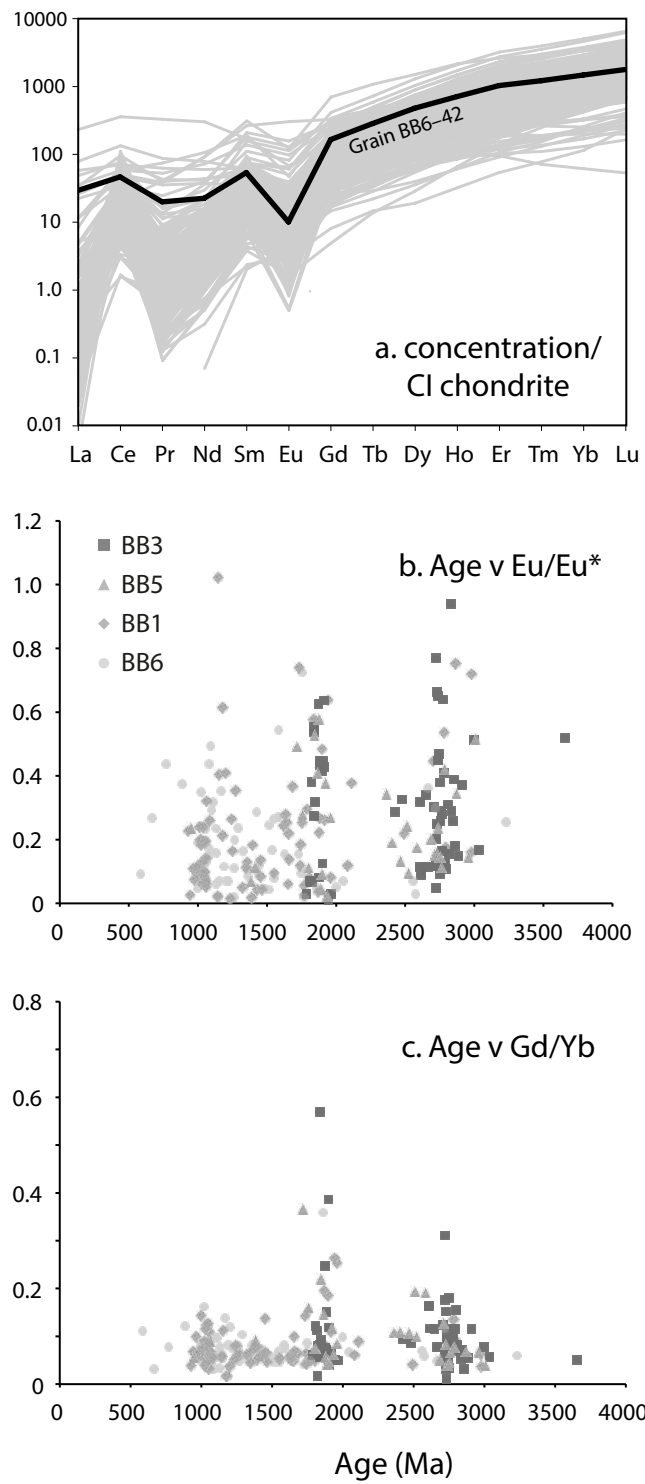


Figure 5

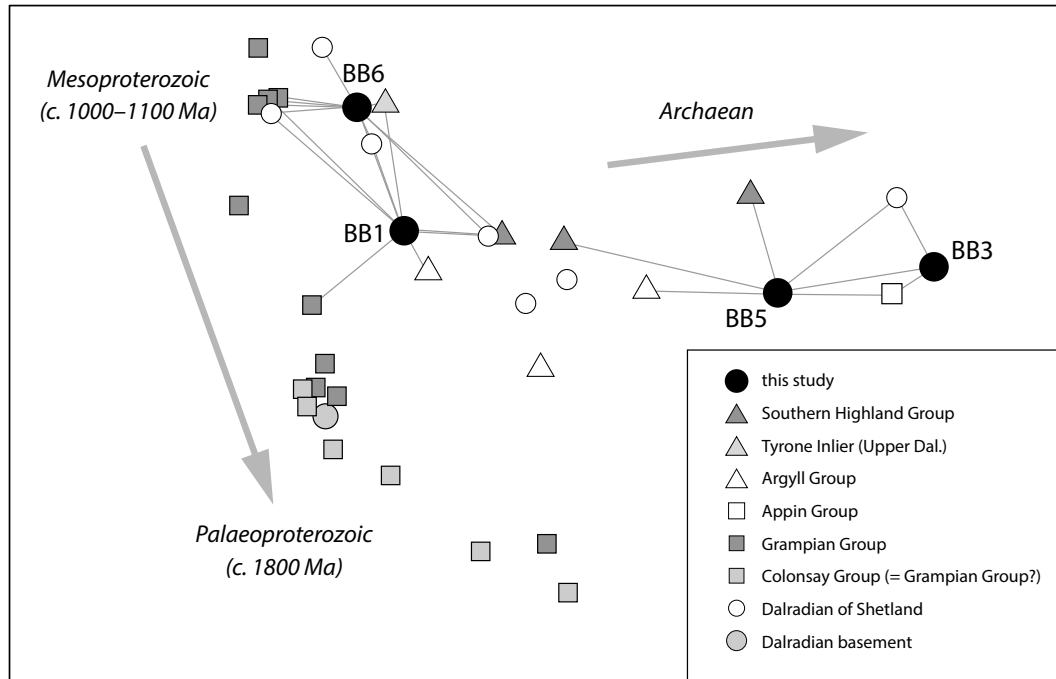


Figure 6

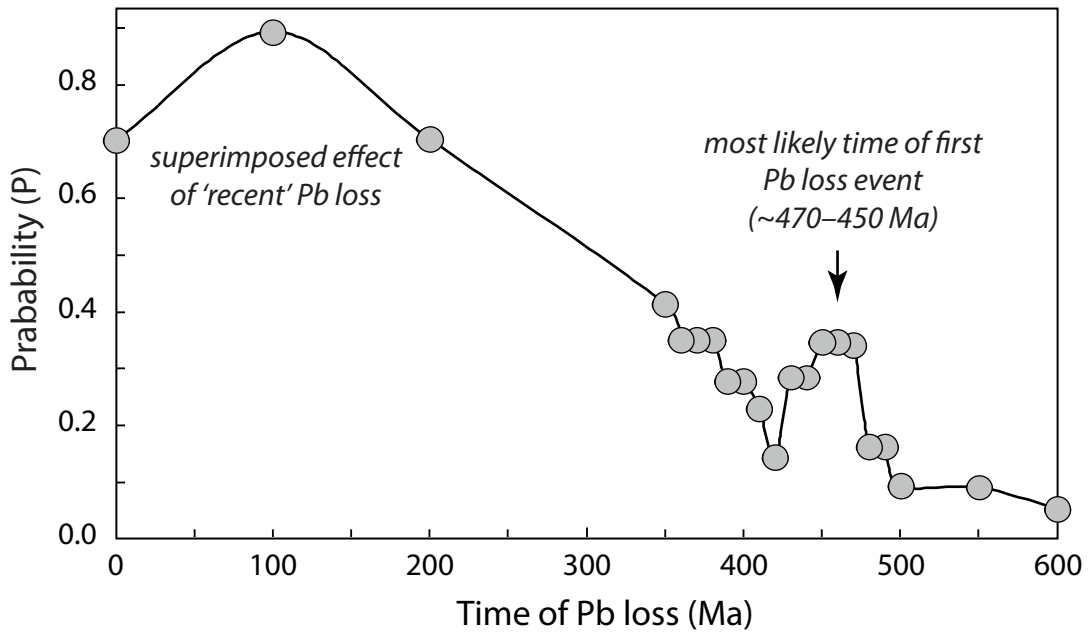
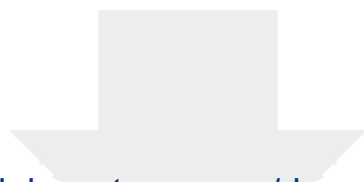


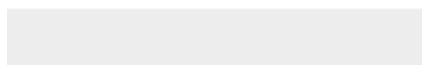
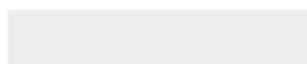
Figure 7



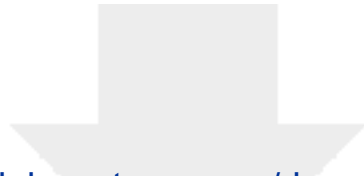
[Click here to access/download](#)

**Dataset**

Table S1.xls



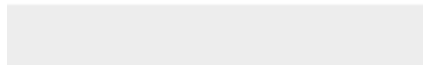





[Click here to access/download](#)

**Dataset**

Table S2.xls





[Click here to access/download](#)

**Dataset**  
**Table S3.xlsx**

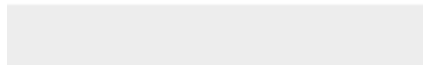


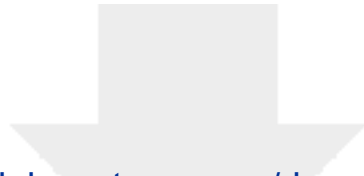


[Click here to access/download](#)

**Supplementary material (not datasets)**

Fig S1 CL images.png





[Click here to access/download](#)

**Supplementary material (not datasets)**

Fig S2 TRACES.pdf

